Fast Voltammetric and Electrochromic Response of Semiconductor Nanocrystal Thin Films†

Philippe Guyot-Sionnest* and Congjun Wang

The University of Chicago, James Franck Institute, 5640 South Ellis Avenue, Chicago, Illinois 60637

Received: November 20, 2002; In Final Form: February 11, 2003

CdSe nanocrystal thin films exhibit stable and quantitative electrochemical responses when treated with cross-linking molecules such as dithiols or diamines. For the first time, a voltammetric response is recorded for the reduction of the nanocrystals with quantitative injection of electrons in the $1S_e$ state. Injection in the $1P_e$ manifold is also achieved as evidenced by spectroscopic measurements. For a 100 nm thick film of 6.2 nm diameter nanocrystals, electrochromic changes are on 100 ms time scales, and remain robust after 10 000 cycles.

Chemically synthesized and monodispersed semiconductor nanocrystals constitute an established and interesting class of chromophores,[1] and the wide range of materials that can be synthesized by the organometallic approach[2] provides many opportunities for optimized spectral response from the UV to the mid-IR. As thin films, the nanocrystals may also become useful in several electrooptic applications. These include photovoltaic panels,[3] light-emitting diodes,[4,5] and lasers.[6] Recently, the electrochromic response was observed [7−9] with new potential applications.

In previous work on the electrochromic response of CdSe nanocrystal thin films,[8] the slow response of the system prevented us from obtaining useful voltammetric data. Although the quantum state occupation was optically observed at a threshold reduction potential, there was large excess current. In recent years, electrochemical characterization of many semiconductor nanocrystals, such as PbS,[10] Si,[11] CdS,[12] and CdSe,[13] has been attempted by differential pulse voltammetry and cyclic voltammetry. Voltammetric features have been observed in these systems, but the experiments have also not provided quantitative measures of electron injection in the quantum states, leaving uncertainty as to the nature of the states in which the charges are injected and the efficiency of the charge injection.

Thin films are probably the most useful for use in electrooptic applications; however, charge flow in a nanocrystal film is possibly affected by many factors. These include electron hopping from nanocrystal to nanocrystal, counter-charge flow into the network, contact resistance to the electrodes, and competitive redox processes that limit the stability of reduced or oxidized nanocrystals.

The use of cross-linkers has been shown in the past to improve the electrical conductance of metal nanocrystal arrays.[14,15] In addition to possible improvement in conduction, the mechanical resilience of the film to charging and discharging could also be strengthened by cross-linking the nanocrystals. For semiconductor nanocrystals, 1,6-hexanedithiol has been used as a cross-linker to bond monolayers of nanocrystals[16] on gold substrates as well as for a scheme to build films monolayer by monolayer.[4,17] Many other cross-linking ligands may be investigated based on thiols, amines, pyridine, or carboxyl groups. We have therefore explored a simple modification of the thin film preparation using cross-linking molecules. The improvements are dramatic and they are reported below.

Experimental Section

The CdSe nanocrystals are prepared according to established organometallic procedures in TOPO/TOP solvents.[18] The nanocrystals are extracted from the reaction mixture with a sequence of precipitation in methanol and redissolution in chloroform. For the thin film preparation, literature procedures are followed.[19] Concentrated solutions of TOPO-capped nanocrystals are prepared in 9:1 (v/v) hexane/octane mixtures. Alternatively, the nanocrystals are recapped by pyridine. This is done by redissolving TOPO/CdSe nanocrystals in pyridine and heating to ∼60 °C for a few minutes. Afterward, the nanocrystals precipitate in hexane and are redissolved in a 1:1 (v/v) methanol/pyridine mixture. All chemicals were purchased from Aldrich and used without further purification.

The working electrodes were either ITO slides (Delta Technologies) or polished platinum disks. The ITO slides were treated with 3-mercaptopropyltrimethoxysilane to provide a binding surface to the nanocrystals. This was done by rinsing the electrodes in chloroform, then spreading the neat silane on the electrode and heating to ∼70 °C for a few minutes, rinsing with chloroform, followed by a bake at 120 °C for 30 min. The polished platinum electrode surface was treated with 1,6-hexanedithiol.

The electrodes and the electrochemical cell are heated to 70 °C prior to introduction in the glovebox. The nanocrystal films were made by depositing a drop of the nanocrystal solution on the electrodes. The drop spreads and dries slowly. The film optical density is determined by the concentration of the solution and ranged between 0.05 and 0.2 at the first absorption peak for all sizes studied. Within minutes of the film appearing dry to the eye, it is dipped in a solution containing the linker molecule at ∼10 mM concentration in the appropriate solvent for 10 s. The solvent is anhydrous methanol for the TOPO-capped CdSe and anhydrous hexane for the pyridine-capped nanocrystals. The excess liquid is left to dry and the electrode is then warmed to 70 °C for 30 min inside the glovebox. After this procedure, the films are insoluble in chloroform, lending support to the notion that the linker molecules can at least partially displace the capping molecules. Afterward, the elec-

† Part of the special issue "Arnim Henglein Festschrift".

* Corresponding author.

10.1021/jp0275084 CCC: $25.00
Published on Web 04/10/2003

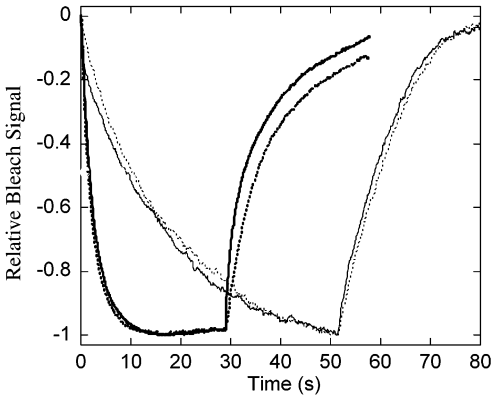

Figure 1. Time trace of the bleach and recovery of 6.2 nm diameter CdSe nanocrystal films on an ITO electrode. The optical signal is measured at 639.5 nm, and all bleach signals are normalized to −1. The solid lines are with a negative potential step followed by returning the potential to 0 V with respect to the Ag pseudo reference. The dotted lines are the same negative potential step followed by disconnecting the electrode. Fine line, TOPO-capped CdSe; heavy line, pyridine-capped CdSe.

trode is placed under vacuum for 30 min. The cross-linking procedure reduces the tendency of the film to exhibit visible cracks. It also significantly reduces the thickness of the film without changing the optical density. For films of TOPO-capped nanocrystals of ∼5.2 nm diameter ranging from 80 to 150 nm thickness, ellipsometric measurements indicate that the film thickness is reduced by 10 to 15% while the index of refraction at 632 nm increases from 1.92 ± 0.01 to 1.99 ± 0.01 after processing with 1,7-heptanediamine. The cell is assembled in the glovebox and filled with anhydrous 0.1 M tetrabutylammonium perchlorate (TBAP) in dimethylformamide (DMF) electrolyte solution. A silver wire is used as a pseudo reference. The potentials shown in the figures are with respect to the Ag wire pseudo-reference. No care was taken to ensure that the reference potential was always consistent. A silver or gold wire is used for the counter electrode.

The cell is taken outside the box for the measurements. Optical spectra are taken with a UV/Vis diode-array spectrometer in transmission for the ITO electrodes and in reflection for the Pt electrode. The infrared spectra are taken with an FTIR spectrometer in reflection from a Pt electrode in the thin layer cell geometry.

Results

When a film of TOPO/CdSe nanocrystals is prepared simply by drying on an ITO or Pt electrode, it exhibits a fairly reproducible electrochromic response; however, the complete color change and recovery takes hundreds of seconds.[8] Moreover, as shown in Figure 1, the recovery takes the same amount of time whether the electrode is simply disconnected or returned to a lower bias. The cathodic current is always much larger than necessary to inject the charges in the nanocrystals, and upon the anodic scan, the current remains positive. Therefore, electrons flow inefficiently from the electrode to the nanocrystal films, and electrons do not even return to the electrode. Presumably, since the bleach recovers, it must be by oxidation from solution. The nature of the oxidation process is not known; however, the bleach recovery rate is increased if the cell is briefly opened to air suggesting that water or oxygen is responsible.

Hoping to improve transport, we investigated shorter capping molecules and found a similar problem. With pyridine, the films

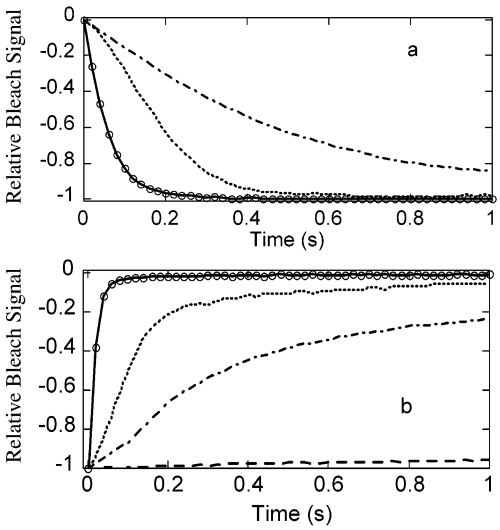

Figure 2. Time trace of the bleach (a) for different films of 6.2 nm CdSe nanocrystals on an ITO electrode after the negative potential step, and recovery (b) after returning the potential to 0 V with respect to the Ag pseudo reference. The optical signal is measured at 639.5 nm, and all bleach signals are normalized to −1. The solid line and data points are for pyridine-capped nanocrystals treated with 1,6-hexanedithiol. The dotted line is for pyridine-capped nanocrystals treated with 4,4′-biphenyldithiol. The dot−dashed line is for TOPO-capped nanocrystals treated with 4,4′-biphenyldithiol. In Figure 2b, the dashed line shows the much slower bleach recovery for a film for pyridine-capped nanocrystals treated with 1,6-hexanedithiol, when the electrode is disconnected.

are quite stable, and the earliest stage of the bleach recovery is faster with the applied potential than with the electrode disconnected, but again, the bulk of the effect occurs at the same rate. Representative data are shown in Figure 1. With a thiophenol cap, the films exhibited behavior similar to that of TOPO-capped nanocrystals and they were overall less stable.

One possible explanation for why charge flows into the film, the cathodic direction, is easier than the reverse, the anodic direction, could be the presence of a barrier close to the electrode. With this in mind, we treated the ITO surface with the surface binding layer provided by the mercapto-silane but found no noticeable improvements. Another possibility is that charge flow in the film competes unfavorably with the oxidation. Upon the cathodic scan, electrons are forced through the film via the potential gradient so that the whole film can still be maintained in a charged state. During the anodic scan, oxidation of nanocrystals could take place spontaneously anywhere in the films, even fairly close to the electrode, effectively isolating the rest of the film before charges can flow back to the electrodes.

Treating the films with cross-linkers dramatically improves the electrochromic kinetics and stability of the films. We also found that previously tested samples can be kept in vials in air for days and that identical electrochromic performances are obtained as long as the samples are baked again to ∼70°C under vacuum for an hour, before insertion into the electrochemical cell, presumably removing adsorbed water.

Figure 2 shows the kinetics of bleach and recovery with films of the order of 100 nm thickness with different preparations and linkers such as 4,4′-biphenyldithiol and 1,6-hexanedithiol. The time scales observed are now 1000-fold faster, with the best response being 100 and 40 ms for 90% bleaching and recovery, respectively, of films with optical densities around 0.15 at the peak exciton. The color switching is easily noticeable by eye. The kinetics in Figure 2 are rather exponential, as for

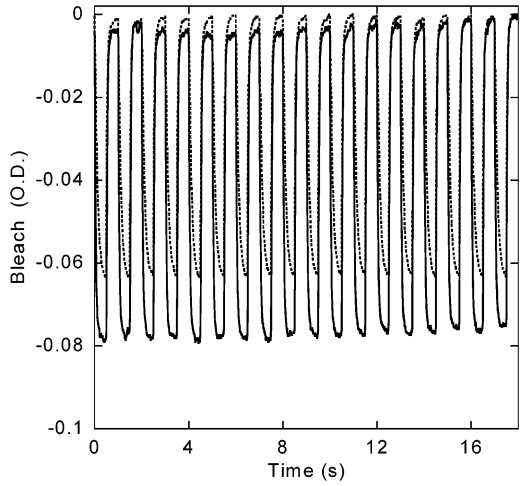

Figure 3. Optical density at 639.5 nm for a 6.2 nm diameter pyridine-capped nanocrystal film cross-linked with 1,6-hexanedithiol on an ITO electrode while cycling the electrode between −0.8 V and −1.4 V with respect to the Ag pseudo reference. The solid line is the electrochromic response of the thin film for the first few cycles. The dotted line is the response after about 3 h and 10 000 cycles.

an RC circuit. They do not show diffusion-controlled behavior in $t^{1/2}$. Similar kinetics are observed with 1,7-heptanediamine linkers applied to TOPO-capped nanocrystal films. In this case, the films retain their fluorescence efficiency. On the other hand, other potential linkers did not lead to any improvements, including pyrazine, 1,4-benzenedithiol, 1,3-dimethylthiolbenzene, or 2,2′-bipyridilamine.

We now focus on results obtained with pyridine-capped nanocrystal films subsequently treated with 1,6-hexanedithiol/methanol solution. The films are stable to repeated cycling. Figure 3 shows the response of the film for short complete cycles before and after 10 000 cycles over 3 h. The film performance is only reduced by 20%, and it is expected that better results would arise with improved airtightness of the cell.

Until this report there had been no evidence of quantitative charge injection in the quantum-confined states of CdSe nanocrystals. The stability of the films and the fast charging and discharging provide the first opportunity to get a quantitative voltammetric response from the nanocrystals. Figure 4 shows the cyclic voltammetry and simultaneous optical density change for a film of 6.2 nm CdSe nanocrystals. The optical signal is obtained with a 639.5 nm diode laser, on the shoulder of the first exciton. It is apparent that the current onset and bleach are synchronous.

To establish the quantitative nature of the charge injection, the ΔOD of the exciton is divided by the integrated surface charge density σ to obtain a value for the one-electron optical cross-section $\alpha = \ln 10 \times \Delta\mathrm{OD} \times e/\sigma$. This is then compared to literature values established by other means. As seen in Figure 4, the derivative of the optical bleach, which should be similar to the charging current associated with injection into the $1S_e$ state, overlaps the peaks or shoulders in the current. A Gaussian is fit to the optical bleach derivative. The same Gaussian curve is then scaled and subtracted from the current to visually obtain the smoothest curve. The area of the Gaussian determines the charge Q associated with charging the $1S_e$ state. By requiring the same charge for both the reduction and oxidation half cycles, Q is equal to 16 ± 1.6 μC. Given the electrode area of 0.85 cm^2, also determined within 10% accuracy, this gives the charge density $\sigma = 19$ μC/cm^2. The maximum optical density change at the exciton peak is 0.072. The optical cross-section per electron at the exciton peak is then 1.4×10^{-15} cm^{-2}. The cross-section of the exciton is twice that value, because two electrons are available for the transitions and it is then 2.8×10^{-15} cm^{-2} with an accuracy of ∼20%. This value compares well to reported numbers ($\sim 3.5 \times 10^{-15}$ cm^{-2} [20] and $\sim 3 \times 10^{-15}$ cm^{-2} [21]) of the peak optical cross-section of the exciton obtained by elemental analysis of colloid samples for particles of similar sizes and polydispersivity. Therefore, the electron injection in the $1S_e$ state of the nanocrystals is quantitative.

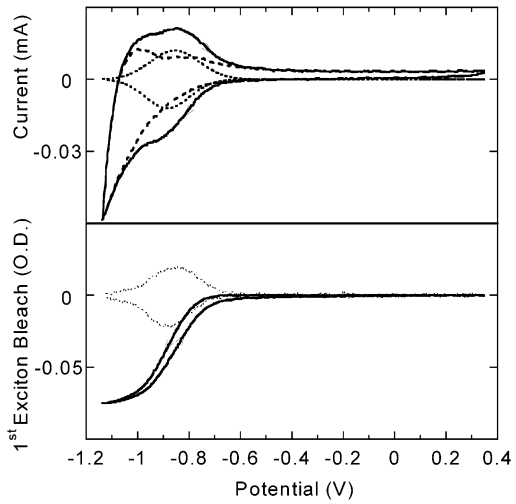

Figure 4. Current and bleach data for a 6.2 nm diameter pyridine-capped CdSe nanocrystal film cross-linked with 1,6-hexanedithiol on an ITO electrode. Scan rate 165 mV/s, electrode area 0.85 cm^2. The potential is with respect to the Ag pseudo reference. For this sample at room temperature the optical density at 639.5 nm is 65% of the optical density at the exciton peak (625 nm). The bleach data is measured at 639.5 nm and divided by this factor to provide the bleach at the exciton peak (solid line). The dotted line in the lower graph is the derivative of the optical bleach. The dotted line in the upper graph is a Gaussian fitted to the optical bleach derivative, and the dashed line is after subtraction of the Gaussian from the current.

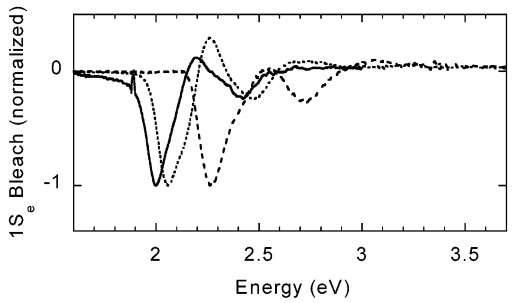

Figure 5. Normalized bleach spectra of thin films of nanocrystals of different diameters: 6.2 nm solid line (−30 °C), 5.2 nm dotted line (20 °C), 3.8 nm dashed line (20 °C).

Figure 5 shows the $1S_e$ bleach spectra for nanocrystals with varying core diameters. As previously reported, three bleach features are noticed.[8] They appear to reflect the 3-fold degeneracy of the valence band structure and to have mostly the character of the heavy-hole (main feature) and light-hole (appearing as a shoulder of the lowest energy feature) and spin−orbit split hole state (upshifted by ∼0.4 eV, the bulk spin−orbit splitting). Compared to previously published detailed excitonic state determination of CdSe nanocrystals,[22] the first two transitions are assigned to $1S_{3/2}-1S_e$ and $2S_{3/2}-1S_e$. However, the third one could be $2S_{1/2}-1S_e$ or $3S_{1/2}-1S_e$, while $1S_{1/2}-1S_e$ is not resolved. The induced absorption between the two features is best observed in the more monodispersed samples. It possibly reflects a shift of the other excitonic transitions, most likely the 1P exciton, upon charging.

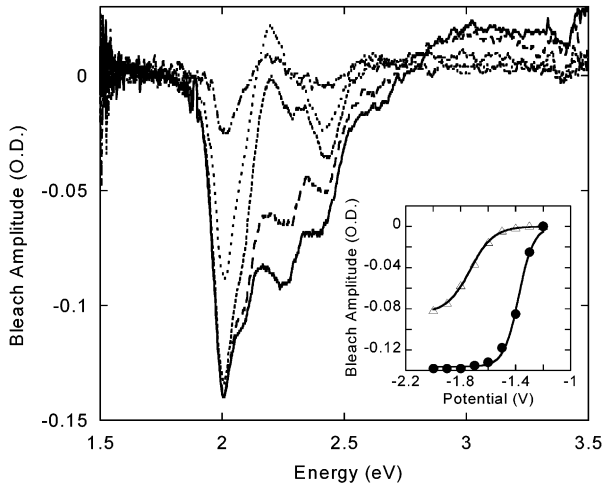

Figure 6. Optical bleach spectra of 6.2 nm pyridine-capped CdSe treated with 1,6-hexanedithiol on ITO, at −50 °C. The potential decreases from −1.3 V to −2 V with respect to the Ag pseudo reference. Spectra are shown for −1.3, −1.4, −1.6, −1.8, and −2 V. The inset shows the bleach amplitudes at 2 eV (filled circles) and 2.3 eV (open triangles) as a function of potential. The solid lines are thermal equilibrium fits with an adjustable "temperature" used as a guide to the eye.

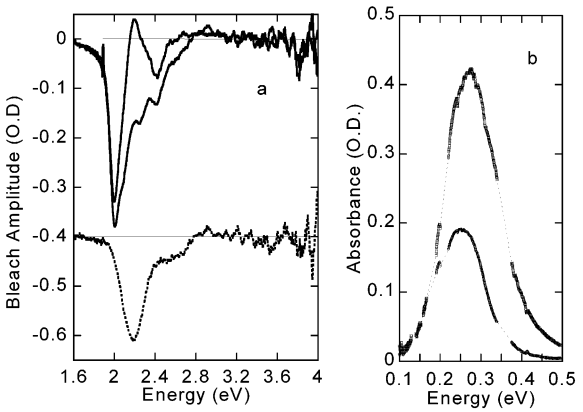

Figure 7. (a) Visible bleach spectra of 6.2 nm pyridine-capped CdSe treated with 1,6-hexanedithiol on a Pt electrode at two potentials (−1.5 V and −1.8 V with respect to the Ag pseudo reference), at −50 °C. The lower bleach spectrum is the difference spectra offset by −0.4 showing the P exciton bleach. (b) Infrared absorption of the same sample at the same potentials. Data are masked (fine dotted connecting lines) where the solvent absorption obscures the signal.

After the $1S_e$ bleach saturates, further bleaching takes place at more negative potentials. Since the films are marginally stable to the more negative potentials due to the increasing oxidation rate, the electrolyte was cooled to slow the spontaneous oxidation and obtain spectroscopic information. The bleach spectra at ~ -50 °C are shown in Figure 6.

The inset in Figure 6 shows the $1S_e$ optical bleach magnitude and a one-electron thermal equilibrium fit $1/(\exp(e(V - V_o)/kT^*) + 1)$ used as a guide to the eye with an effective temperature of 620 K or 53 meV. The excess width must arise from the inhomogeneous size distribution. In addition, the charging energy may play a role since the $1S_e$ state can accommodate two electrons. A fit of the bleach amplitude as a function of the potential can indeed be obtained with a Gaussian inhomogeneous distribution of 50 meV and a charging energy of 70 meV. Such a charging energy is plausible[20] as it would be the one-electron charging energy of a 6 nm diameter conducting sphere in an effective dielectric environment with $\epsilon = 7$. However, we do not know the effective dc dielectric constant of the films in the electrolyte.

The difference between the $1S_e$ bleach spectrum (peak at 2 eV) and bleach at more negative potentials shows mostly two features. The first well-defined resonance at 2.2 eV is attributed to $1P_{3/2}-1P_e$.[22] The second feature at 2.6 eV, upshifted again by the spin−orbit coupling energy, is attributed to $1P^{so}{}_{1/2}-1P_e$.[22] The inset shows that the charge injection into the $1P_e$ state is ~0.35 V more negative than the injection into the $1S_e$ state and occurs over an even broader potential range.

The occupation of the $1P_e$ state is also observed for the first time in the infrared intraband spectrum. As shown in Figure 7, the overall infrared intensity of the intraband transition greatly increases upon electron injection into the $1P_e$ state, in proportion to the bleach strength; in addition, the intraband absorption is noticeably wider and slightly blue-shifted compared to the $1S_e-1P_e$ transition. In the constant effective mass and spherical box approximation, the $1P_e-1D_e$ energy is 30% larger than $1S_e-1P_e$. It is therefore not surprising that the spectra appear in the same range. Note that the energy of the $1S_e-1P_e$ transition is 0.25 eV. Yet the visible bleach spectra show that the energy of the 1P exciton is only 0.2 eV larger than the 1S exciton. This discrepancy may be attributed to the Coulomb energy stabilization of the exciton.

Fluorescence data in these cross-linked films are not discussed here. They are similar to data previously reported:[8] quenching of the fluorescence takes place upon electron injection, but the fluorescence recovery occurs on a much longer time scale than the electron extraction.

In summary, thin films of CdSe nanocrystals show greatly improved electrochemical stability and speed when a cross-linking procedure is applied. Furthermore, the enhanced speed and stability allows the injection of electrons into higher electronic states, with corresponding tunable chromatic changes. The cross-linking procedure used here is elementary. Optimized ligands and film preparation should allow further improvements. The combined use of high-surface-area electrodes[23] may provide deeper chromatic response.[24] Further enhancement in stability and speed are thus likely, leading to the development of semiconductor nanocrystals for practical visible and infrared electrochromic devices or other devices based on the electrochemical response.

Acknowledgment. This work was funded by the U.S. National Science Foundation (NSF) under Grant DMR-0108101. The authors made use of the MRSEC Shared Facilities supported by NSF under Grant DMR-9400379.

References and Notes

(1) Steigerwald, M. L.; Brus, L. E. *Annu. Rev. Mater. Sci.* **1989**, *19*, 471.

(2) Murray, C.B.; Norris, D. J.; Bawendi, M. G. *J. Am. Chem. Soc.* **1993**, *115*, 8706.

(3) Greenham, N. C.; Peng, X. G.; Alivisatos, A. P. *Phys. Rev. B* **1996**, *54*, 17628.

(4) Colvin, V. L.; Schlamp, M. C.; Alivisatos, A. P. *Nature* **1994**, *370*, 354.

(5) Dabbousi, B. O.; Bawendi, M. G.; Onitsuka, O.; Rubner, M. F. *Appl. Phys. Lett.* **1995**, *66*, 1316.

(6) Eisler, H. J.; Sundar, V. C.; Bawendi, M. G.; Walsh, M.; Smith, H. I.; Klimov, V. *Appl. Phys. Lett.* **2002**, *80*, 4614.

(7) Wang, C.; Shim, M.; Guyot-Sionnest, P. *Science* **2001**, *291*, 2390.

(8) Wang, C.; Shim, M.; Guyot-Sionnest, P. *Appl. Phys. Lett.* **2002**, *80*, 4.

(9) Woo, W. K.; Shimizu, K. T.; Jarosz, M. V.; Neuhauser, R. G.; Leatherdale, C. A.; Rubner, M. A.; Bawendi, M. G. *Adv. Mater.* **2002**, *14*, 68.
(10) Chen, S.; Trax, L. A.; Sommers, J. M. *Chem. Mater.* **2000**, *12*, 3864.
(11) Ding, Z. F.; Quinn, B. M.; Haram, S. K.; Pell, L. E.; Korgel, B.A.; Bard, A. J. *Science* **2002**, *296*, 1293.
(12) Haram, S. K.; Quinn, B. M.; Bard, A. J. *J. Am. Chem. Soc.* **2001**, *123*, 8860.
(13) Myung, N.; Ding, Z.; Bard, A. J. *Nano Lett.* **2002**, *2*, 1315.
(14) Andres, R. P.; Bielefeld, J. D.; Henderson, J. I.; Janes, D. B.; Kolagunta, V. R.; Kubiak, C., P.; Mahoney, W. J.; Osifchin, R. G. *Science* **1996**, *273*, 1690.
(15) Zamborini, F. P.; Leopold, M. C.; Hicks, J. F.; Kulesza, P. J.; Malik, M. A.; Murray, R. W. *J. Am. Chem. Soc.* **2002**, *124*, 8958.
(16) Colvin, V. L.; Goldstein, A. N.; Alivisatos, A. P. *J. Am. Chem. Soc.* **1992**, *114*, 5221.
(17) Hu, K.; Brust, M.; Bard, A. J. *Chem. Mater.* **1998**, *10*, 1160.
(18) Murray, C. B.; Kagan, C. R.; Bawendi, M. G. *Annu. Rev. Mater. Sci.* **2000**, *30*, 545.
(19) Leatherdale, C. A.; Kagan, C. R.; Morgan, N. Y.; et al. *Phys. Rev. B* **2000**, *62*, 2669.
(20) Shim, M.; Guyot-Sionnest, P. *J. Chem. Phys.* **1999**, *111*, 6955.
(21) Leatherdale, C. A.; Woo, W. K.; Mikulec, F. V.; Bawendi, M. G. *J. Phys. Chem. B* **2002**, *106*, 761.
(22) Norris, D. J.; Bawendi, M. G. *Phys. Rev. B* **1996**, *53*, 16338.
(23) O'Reagan, B.; Grätzel, M. *Nature* **1991**, *353*, 737.
(24) Cummins, D.; Boschloo, G.; Ryan, M.; Corr, D.; Rao, S. N.; Fitzmaurice, D. *J. Phys. Chem. B* **2000**, *104*, 11449.